CHEMISTRY

Gas-phase detection of oxirene

Jia Wang[1,2], Joshua H. Marks[1,2], Andrew M. Turner[1,2], Alexander M. Mebel[3]*, André K. Eckhardt[4]*, Ralf I. Kaiser[1,2]*

Oxirenes—highly strained 4π Hückel antiaromatic organics—have been recognized as key reactive intermediates in the Wolff rearrangement and in interstellar environments. Predicting short lifetimes and tendency toward ring opening, oxirenes are one of the most mysterious classes of organic transients, with the isolation of oxirene (*c*-C_2H_2O) having remained elusive. Here, we report on the preparation of oxirene in low-temperature methanol-acetaldehyde matrices upon energetic processing through isomerization of ketene (H_2CCO) followed by resonant energy transfer of the internal energy of oxirene to the vibrational modes (hydroxyl stretching and bending, methyl deformation) of methanol. Oxirene was detected upon sublimation in the gas phase exploiting soft photoionization coupled with a reflectron time-of-flight mass spectrometry. These findings advance our fundamental understanding of the chemical bonding and stability of cyclic, strained molecules and afford a versatile strategy for the synthesis of highly ring-strained transients in extreme environments.

INTRODUCTION

Since the very first suggestion of oxirenes as highly strained 4π heterocyclic anti-aromatic molecules by Berthelot more than 150 years ago (*1*), oxirenes have emerged as key reactive intermediates in preparative organic synthesis (*2*), physical organic chemistry (*3*), and theoretical chemistry (*4*, *5*). The high ring strain and the antiaromatic character of oxirenes is well documented in the literature (*2*, *6*, *7*). Envisaging the short lifetimes (*8*, *9*) and high reactivity (*10*, *11*) of these transient molecules along with their critical role in the Wolff rearrangement (conversion of α-diazo ketones into ketenes) (*4*, *12*–*14*), oxirenes are one of the most mysterious classes of organic reactive intermediates, with its prototype—oxirene (oxacyclopropene, **1**, *c*-C_2H_2O; Fig. 1)—still being elusive. So far, only four substituted oxirenes have been isolated in low-temperature matrices [dimethyloxirene (*10*); bis-(trifluoromethyl)- and perfluoromethylethyl-oxirene (*15*)] or through neutralization-reionization mass spectrometry (methyloxirene) (*11*); these species represent benchmarks for testing fundamental concepts of Hückel (anti) aromaticity (*7*, *16*–*18*).

Whether oxirene (**1**) represents a true local minimum or a transition state has remained a notorious case of an unsolved computational "existence problem" (*7*, *19*, *20*). Ultimately, functionals such as the revision of Becke's hybrid functional (B97-2) and the hybrid functional of Perdew, Burke, and Ernzerhof (PBE0) predicted oxirene (**1**) as a local minimum but less stable by 341 kJ mol^{-1} with respect to ketene (**2**, H_2CCO) (*7*, *18*); this agrees nicely with the earlier study at the single, double, and perturbative triple excitation coupled-cluster [CCSD(T)] level of theory (*17*, *21*). A recent study (*20*) at the CCSD(T)/def2-TZVPP//B3LYP-D3/def2-TZVP level suggested the existence of a nonsymmetrical (C_s distorted) pseudocyclic structure with a long (167.3 pm) and short (137.6 pm) carbon-oxygen single bond as a local minimum; this structure was proposed to interconvert into the degenerate structure through a low-lying C_{2v}-symmetric cyclic transition state positioned about 1 kJ mol^{-1} above the distorted local minimum. This result is not supported by any other previous (*7*, *9*, *20*) or present geometry optimization at the higher ab initio CCSD(T) level of theory (Results). However, despite the computational prediction that oxirene (*c*-C_2H_2O, **1**) can be "made" in the laboratory, all experimental attempts involving, e.g., photochemistry of vinylene carbonate (1,3-dioxol-2-one, $C_3H_2O_3$) in an argon matrix (*22*), gas-phase neutralization of the oxirene radical cation (*23*), the identification of oxirene (**1**) as a reactive intermediate in the isomerization of ketene (**2**) to ethynol (**4**, HCCOH) in an argon matrix (*24*), and strained organic precursors such as diazoacetaldehyde (HCN_2CHO) (*25*, *26*), have failed so far. This is likely due to the previous difficulties in transferring the internal energy from the newly formed, vibrationally excited oxirene (**1**) to the surrounding medium (gas-phase third body collider, matrix molecules) on time scales competing with its decomposition and/or isomerization to ketene (**2**) or ethynol (**4**).

Here, we report the first laboratory synthesis and detection of oxirene (*c*-C_2H_2O, **1**) in low-temperature ices of methanol (CH_3OH) and acetaldehyde (CH_3CHO) exposed to energetic electrons at 5 K. Using the vacuum ultraviolet (VUV) photoionization reflectron time-of-flight mass spectrometry (PI-ReTOF-MS), oxirene (**1**) and its isomer ketene (**2**) are identified through isomer-specific photoionization in the gas phase during the temperature-programmed desorption (TPD) phase of the irradiated ices. Combined with isotopic labeling of the reactants, intimate insights into the formation mechanism of oxirene (**1**) via isomerization of ketene (**2**), which is prepared in situ via molecular hydrogen loss from acetaldehyde, are obtained with internally excited oxirene (**1**) stabilized under matrix isolation conditions through resonances with the OH stretching and bending, CH_3 deformation, and/or CO stretching modes of methanol. Upon sublimation of the matrix, oxirene molecules (**1**) are photoionized in the gas-phase isomer-selectively exploiting single photon ionization (PI) and detected with a ReTOF-MS (*27*). The preparation and detection of oxirene (**1**) along with its isotopologues reveals its gas-phase stability with lifetimes of at least 8 ± 2 μs despite a barrier of only 22 kJ mol^{-1} toward

[1]W. M. Keck Research Laboratory in Astrochemistry, University of Hawaii at Manoa, Honolulu, HI 96822, USA. [2]Department of Chemistry, University of Hawaii at Manoa, Honolulu, HI 96822, USA. [3]Department of Chemistry and Biochemistry, Florida International University, Miami, FL 33199, USA. [4]Lehrstuhl für Organische Chemie II, Ruhr-Universität Bochum, Bochum 44801, Germany.
*Corresponding author. Email: mebela@fiu.edu (A.M.M.); andre.eckhardt@rub.de (A.K.E.); ralfk@hawaii.edu (R.I.K.)

isomerization to ethynol (**4**) (*28*). These findings advance our fundamental knowledge of the exotic chemistry, chemical bonding, and unusual preparation of highly strained molecules such as oxirene (**1**), thus affording an elegant route for the synthesis of hitherto elusive transients through resonant energy transfer of internal energy from the newly formed molecule to the vibration modes of the surrounding matrix (methanol). The strategy of "tuning" the matrix medium to match the resonance conditions with (high energy) vibrational modes of the target molecule to be synthesized will not only assist in preparing "elusive" molecules such as methanetriol [$CH(OH)_3$] organic chemists have attempted to isolate for decades but also predict that oxirene (**1**) may also be formed in methanol-rich interstellar ices in cold molecular clouds from acetaldehyde; hence, upon sublimation in star-forming regions, oxirene (**1**) represents a worthwhile astronomical target to be searched for in the gas phase by radio telescopes such as the Atacama Large Millimeter/submillimeter Array (ALMA).

RESULTS

The methanol-acetaldehyde ices were monitored during electron irradiation at 5 K via Fourier transform infrared (FTIR) spectroscopy (figs. S1 and S2). Absorptions emerged at 2129, 1840 , 1306, and 1199 cm^{-1} (fig. S2 and tables S1 and S2), which are linked to the CO stretch (2129 cm^{-1}) of ketene (**2**) and/or carbon monoxide (CO), the acetyl radical [$CH_3\dot{C}O$, ν(C═O)], the deformation mode of methane (CH_4; ν_4), and the hydroxymethyl radical ($\dot{C}H_2OH$; ν_4), respectively (*29*, *30*). Note that absorptions at 2087 and 2066 cm^{-1} emerged after irradiation in the CH_3OH-$^{13}CH_3{}^{13}CHO$ ice (fig. S3 and table S3); these absorptions agree well with previous measurements in which the absorption bands of ^{13}CO at 2091 cm^{-1} and ketene-$^{13}C_2$ ($H_2{}^{13}C{}^{13}CO$) at 2071 cm^{-1} were observed from proton irradiated H_2O-$^{13}C_2H_2$ ice at 18 K (*31*). Therefore, these two absorptions can be linked to ^{13}CO and ketene-$^{13}C_2$, respectively. The calculated absorptions of oxirene (**1**) strongly overlap with those of the precursor molecules (table S4) including the broad O—H stretching (3020 to 3600 cm^{-1}; ν_1) and bending (1420 cm^{-1}; ν_6) modes, the C—H bending mode (1455 cm^{-1}; ν_5), and the C—O stretching mode (1030 cm^{-1}; ν_8) of methanol (*29*) and the stretching mode of the carbonyl moiety (1718 cm^{-1}; ν_4) of acetaldehyde (*30*); consequently, infrared spectroscopy cannot identify the elusive oxirene (**1**), and an alternative detection technique is imperative.

The PI-ReTOF-MS approach represents an elegant technique for identifying gas-phase molecules isomer-selectively during the TPD phase via soft photoionization based on their mass-to-charge ratios (*m*/*z*) and distinct adiabatic ionization energies (IEs) (*27*). Considering the computed IEs of the C_2H_2O isomers (Fig. 1 and table S5), a photon energy of 9.70 eV was selected first to ionize oxirene (**1**, IE = 8.58 to 8.66 eV) and ketene (**2**, IE = 9.53 to 9.61 eV) but neither oxiranylidene [**3**, $CH_2(CO)$; IE = 9.77 to 9.85 eV] (*32*) nor ethynol (**4**, IE = 9.95 to 10.03 eV). Note that the nondetection of triplet formylcarbene (**5**, IE = 6.30 to 6.38 eV) will be discussed below. Thereafter, we reduced the photon energy to 9.20 eV to only ionize oxirene (**1**) but not ketene (**2**) (Fig. 1). At 9.70 eV, the TPD profile of ion counts at *m*/*z* = 42 from exposed CH_3OH-CH_3CHO ice (Fig. 2A) reveals three prominent sublimation events centered at 103, 112, and 128 K. Accounting for the molecular mass of the reactants, signal at *m*/*z* = 42 could belong to the

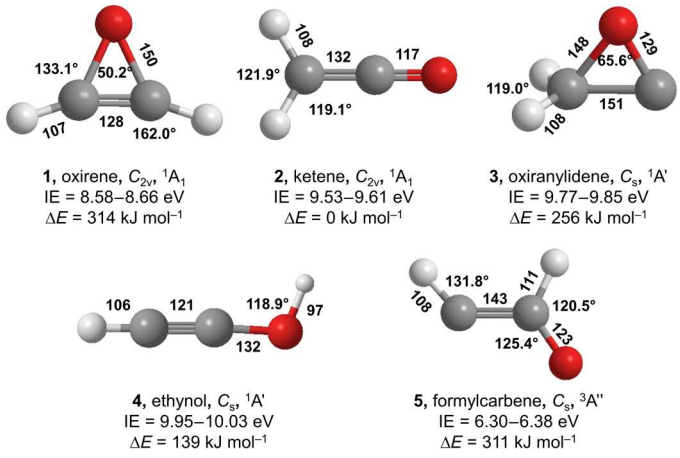

1, oxirene, C_{2v}, $^1A_1$
IE = 8.58–8.66 eV
ΔE = 314 kJ mol^{-1}

2, ketene, C_{2v}, $^1A_1$
IE = 9.53–9.61 eV
ΔE = 0 kJ mol^{-1}

3, oxiranylidene, C_s, $^1A'$
IE = 9.77–9.85 eV
ΔE = 256 kJ mol^{-1}

4, ethynol, C_s, $^1A'$
IE = 9.95–10.03 eV
ΔE = 139 kJ mol^{-1}

5, formylcarbene, C_s, $^3A''$
IE = 6.30–6.38 eV
ΔE = 311 kJ mol^{-1}

Fig. 1. Structures of C_2H_2O isomers. Bond length (in picometers), angles (in degrees), point groups, and electronic ground states are shown. The atoms are color-coded in white (hydrogen), gray (carbon), and red (oxygen). Ranges of computed adiabatic IEs corrected for the electric field effect and relative energies (ΔE) calculated at the CCSD(T)/CBS//CCSD(T)/aug-cc-pVTZ with anharmonic corrections to the zero-point vibrational energy (ZPVE).

molecular formulae C_3H_6 and C_2H_2O. The formula C_3H_6 can account for two isomers: cyclopropane (*c*-C_3H_6, IE = 9.86 ± 0.04 eV) and propene (CH_3CHCH_2, IE = 9.73 ± 0.01 eV) (*33*). To determine the molecular formula(e), experiments with isotopically labeled reactants were conducted. The sublimation profile at *m*/*z* = 42 obtained in the CH_3OH-CH_3CHO ice (Fig. 2A) was shifted by 2 atomic mass units (amu) to *m*/*z* = 44 in CH_3OH-CD_3CHO (Fig. 2B), CD_3OH-CD_3CDO ices (Fig. 2C), and CH_3OH-$^{13}CH_3{}^{13}CHO$ ices (Fig. 2D), supporting the existence of two carbon and two hydrogen atoms along with one oxygen atom confirming the molecular formula C_2H_2O. Since oxiranylidene (**3**) and ethynol (**4**) cannot be ionized at 9.70 eV, the sublimation events in the CH_3OH-CH_3CHO ices must be linked to oxirene (**1**) and/or ketene (**2**). Upon tuning to 9.20 eV, which is below the IE of ketene (**2**, IE = 9.53 to 9.61 eV), the first two sublimation events centered at 103 and 112 K vanish; this indicates that both peaks originate from ketene (**2**). The identification of ketene (**2**) confirms the FTIR results above, in which the absorption at 2066 cm^{-1} in the irradiated CH_3OH-$^{13}CH_3{}^{13}CHO$ ice was assigned to ketene-$^{13}C_2$ ($H_2{}^{13}C{}^{13}CO$). Previous studies demonstrated a sublimation temperature of ketene (**2**) of 100 ± 2 K (*28*, *34*), which is consistent with the lowest temperature sublimation event of 103 K. The second sublimation event at 112 K can be associated with the phase transition from amorphous to the crystalline phase of methanol covering a temperature range from 100 to 120 K (*35*). The signal centered at 129 K still prevails in the irradiated CH_3OH-CH_3CHO (*m*/*z* = 42) *and* isotopically labeled ices (*m*/*z* = 44; Fig. 2, A to D, bottom) at 9.20 eV—a photon energy at which only oxirene (**1**, IE = 8.58 to 8.66 eV) can be ionized. Therefore, the signal at the sublimation profile peaking at 128 K can solely be linked to oxirene (**1**), which —once again—is supported through the presence of signal at *m*/*z* = 44 in all isotopically labeled experiments (Fig. 2, B to D, bottom). Note that the broad sublimation events from 145 to 200 K in the CD_3OH-CD_3CDO (Fig. 2C) and CH_3OH-$^{13}CH_3{}^{13}CHO$ ices (Fig. 2D) originate from $C_2H_2DO^+$ (*m*/*z* = 44) and $^{13}CCH_3O^+$ (*m*/*z* = 44), respectively. Lowering the photon energy

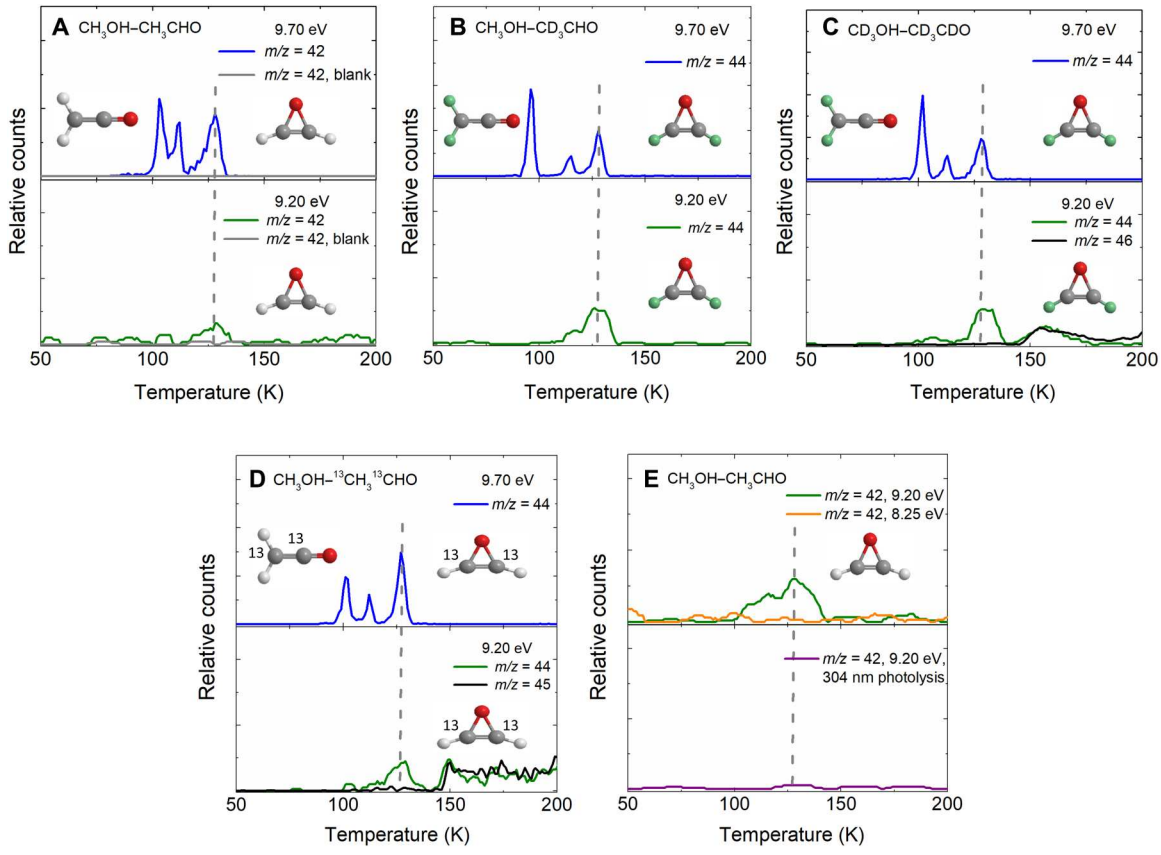

Fig. 2. PI-ReTOF-MS data recorded during the TPD phase of mixture ices. TPD desorption profiles of ion signals of interest detected at 9.70 eV (top) and 9.20 eV (bottom) in four irradiated (20 nA, 15 min) ice mixtures: (**A**) $C_2H_2O^+$ (m/z = 42) in CH_3OH-CH_3CHO ice; (**B**) $C_2D_2O^+$ (m/z = 44) in CH_3OH-CD_3CHO ice; (**C**) $C_2D_2O^+$ (m/z = 44) in CD_3OH-CD_3CDO ice; (**D**) $^{13}C_2H_2O^+$ (m/z = 44) in CH_3OH-$^{13}CH_3{}^{13}CHO$ ice. The sublimation events from 145 to 200 K in CD_3OH-CD_3CDO ice (C, bottom) and CH_3OH-$^{13}CH_3{}^{13}CHO$ ice (D, bottom) are due to $C_2H_2DO^+$ (m/z = 44) and $^{13}CCH_3O^+$ (m/z = 44), respectively. (**E**) TPD profiles of ion signal for m/z = 42 in irradiated (20 nA, 60 min) CH_3OH-CH_3CHO ices recorded at photoionization energy of 9.20 and 8.25 eV (top). For the photolysis experiment at 9.20 eV, the ice was photolyzed at 304 nm after the synthesis via electron exposure (bottom). The dashed line indicates the sublimation peak of oxirene. The atoms are color-coded in white (hydrogen), light green (deuterium), gray (carbon), and red (oxygen).

further to 8.25 eV, which is below the IE of all C_2H_2O isomers, eliminates all ion counts at 129 K, thus providing additional evidence that this event results from oxirene (**1**) (Fig. 2E, top). Blank experiments were also conducted at 9.70 and 9.20 eV under identical conditions preventing the exposure of the ices to ionizing radiation. No ions at m/z = 42 were detected (Fig. 2A, solid gray lines), demonstrating that the identified species are connected to the irradiation of the ices but not due to ion-molecule reactions in the gas phase.

To further confirm the formation of oxirene (**1**), we conducted an ultraviolet (UV) photolysis experiment (*36*, *37*) of oxirene (**1**). The CH_3OH-CH_3CHO ice was first irradiated with energetic electrons to produce oxirene (**1**), which was subsequently photolyzed with 304 nm at 20 mW for 5 hours, an absorption that is uniquely linked to oxirene (**1**) but to none of the other isomers (fig. S4). As evident from the TPD profile recorded after the photolysis, the sublimation peak at 129 K vanishes, and no ions at m/z = 42 remain (Fig. 2E, bottom). This finding provides compelling evidence on the radiation-induced formation and subsequent photolytic destruction of oxirene (**1**).

Having demonstrated the detection of oxirene (**1**) and ketene (**2**), we are now shifting our attention to their formation mechanisms. After electron irradiation, the infrared feature at 1840 cm^{-1} in the ice at 5 K (figs. S1 and S2) is linked to the acetyl radical ($CH_3\dot{C}O$), which represents the dominant product of the unimolecular decomposition of acetaldehyde via carbon-hydrogen single-bond rupture (*38*); this process is endoergic by 377 kJ mol^{-1} (*30*) and can be supplied by the impinging energetic electrons. Note that the vinoxy radical ($\dot{C}H_2CHO$) can also be produced via an endoergic (411 kJ mol^{-1}) atomic hydrogen loss from acetaldehyde (*39*). Ketene (**2**) may form via the removal of one hydrogen atom from the acetyl ($CH_3\dot{C}O$) or vinoxy radical ($\dot{C}H_2CHO$) with reaction endoergicities of 177 or 150 kJ mol^{-1} (fig. S5A) (*40*), respectively. Alternatively, ketene (**2**) can be prepared in one step via the elimination of molecular hydrogen through a transition state located 337 kJ mol^{-1} above the reactant (acetaldehyde) (*41*). Both mechanisms via two successive atomic hydrogen losses and/or molecular hydrogen elimination are also confirmed in ices carrying acetaldehyde-d_3 (CD_3CHO; m/z = 47), acetaldehyde-d_4 (CD_3CDO; m/z = 48), and acetaldehyde-$^{13}C_2$ ($^{13}CH_3{}^{13}CHO$; m/z = 46) through the identification of ketene-d_2 (D_2CCO, m/z = 44), ketene-d_2 (D_2CCO, m/z = 44), and ketene-$^{13}C_2$ ($H_2{}^{13}C{}^{13}CO$, m/z = 44), respectively (fig. S5, B to D). Therefore, these findings

demonstrate that ketene (**2**) originates from acetaldehyde along with its isotopically substituted species. Oxirene (**1**) can then be formed via electron-induced isomerization of ketene (**2**) through a barrier of 353 kJ mol^{-1}. To aid the stabilization and hence transfer of internal energy from oxirene (**1**), the internal energy can be transferred resonantly from the symmetric CH stretching (ν_1) and the combination modes of oxirene to the OH stretching (ν_1) and bending (ν_6), CH_3 deformation (ν_5), and/or CO stretching (ν_8) modes of methanol (Fig. 3 and table S4). These results are also obtained in methanol–acetaldehyde-d_3 ice (fig. S6 and table S6), methanol-d_3–acetaldehyde-d_4 ice (fig. S7 and table S7), and methanol–acetaldehyde-$^{13}C_2$ ice (fig. S8 and table S8). Therefore, the presence of a methanol matrix is essential to the preparation and stabilization of oxirene (**1**) due to their overlapping vibrational modes and hence the possibility of resonant energy transfer. The critical role of methanol as an energy transfer medium is also supported through the lack of any detection of oxirene (**1**) in pure acetaldehyde ices under otherwise identical conditions (fig. S9).

The detection of oxirene could have been thwarted by the existence of a singlet formylcarbene intermediate (HCOCH, **6**) in its vicinity. CCSD(T)/6-311G(df,p) calculations by Scott *et al.* (*13*) predicted singlet formylcarbene (**6**) as a local minimum on the C_2H_2O potential energy surface (PES). This species was suggested to be 2.0 kJ mol^{-1} lower in energy than oxirene (**1**), with a barrier separating oxirene (**1**) and formylcarbene (**6**) of only 1.9 kJ mol^{-1}. Subsequent calculations of Guan *et al.* (*42*) suggested that singlet formylcarbene (**6**) is an excited electronic state of formylcarbene, with the ground triplet state lying 8.4 kJ mol^{-1} lower in energy as computed at the CCSD(T)/cc-pVQZ level of theory. If this were the case, under our experimental conditions in the ice matrix, oxirene would have avoided detection by rapidly isomerizing to singlet formylcarbene (**6**), which in turn would have undergone an intersystem crossing (ISC) to triplet formylcarbene (**5**); ISC is expected to be very efficient in the condensed phase. However, no triplet formylcarbene (**5**), which has an adiabatic IE of 6.30 to 6.38 eV, was detected. To rationalize the experimental detection of oxirene (**1**), here, we revisited the oxirene (**1**) → ketene (**2**) isomerization pathway at the CCSD(T)/aug-cc-pVTZ level of theory including harmonic zero-point vibrational energy (ZPVE) obtained by the same method, with anharmonic corrections evaluated at the PBE0/aug-cc-pVTZ level (Fig. 4).

One can see that at this theoretical level, singlet formylcarbene (**6**) still optimizes as a local minimum, but the inclusion of ZPE lifts its energy above the energy of transition state separating it from oxirene (**1**), which is computed to be 3.7 kJ mol^{-1} more stable than singlet formylcarbene (**6**). Thus, the latter is unlikely to represent a stationary structure on the PES, thus making the ISC to triplet formylcarbene (**5**) unlikely. The electronic vertical singlet-triplet gap in oxirene is 270.8 kJ mol^{-1}, which is also reflected in the T1 diagnostic value of 0.0142. However, the T1 diagnostics of singlet formylcarbene (**6**) along with the transition states TS1 and TS2 (Fig. 4, T1 > 0.02) indicate that the CCSD(T) energies of these structures may not be "gold-standard" accurate as multireference effects are notable (*43*). Unexpectedly, the multireference character of formylcarbene has not been considered in previous computational studies. Therefore, we recomputed single-point energies of all coupled-cluster stationary structures on the PES using the multireference perturbation theory CASPT2 (*44*, *45*) with an active space including 16 electrons and 14 orbitals, which is the full valence active space. As evident from Fig. 4, the singlet formylcarbene (**6**) is positioned 20.8 kJ mol^{-1} above oxirene (**1**) and 2.7 kJ mol^{-1} higher in energy than TS1. Moreover, the CASPT2 (16,14) calculations in the complete basis set (CBS) limit show that triplet formylcarbene (**5**) lies 1.2 kJ mol^{-1} above oxirene. It is important to note that the inclusion of diffuse basis functions in the basis set is critical to resolve this issue, e.g., at the CASPT2 (16,14)/cc-pVTZ//CCSD(T)/aug-cc-pVTZ level, singlet formylcarbene (**6**) is only 0.6 kJ mol^{-1} higher in energy than oxirene (**1**). In addition, the convergence of the CASPT2 energies to the CBS limit is enhanced for the aug-cc-pVxZ (x = T, Q) basis sets as compared to cc-pVxZ (table S9). Essentially, the nonexistence of singlet formylcarbene (**6**) (*46*) as a stationary structure and a lower stability triplet formylcarbene (**5**) than predicted by the earlier theoretical calculations allow for the experimental detection of oxirene in the present study.

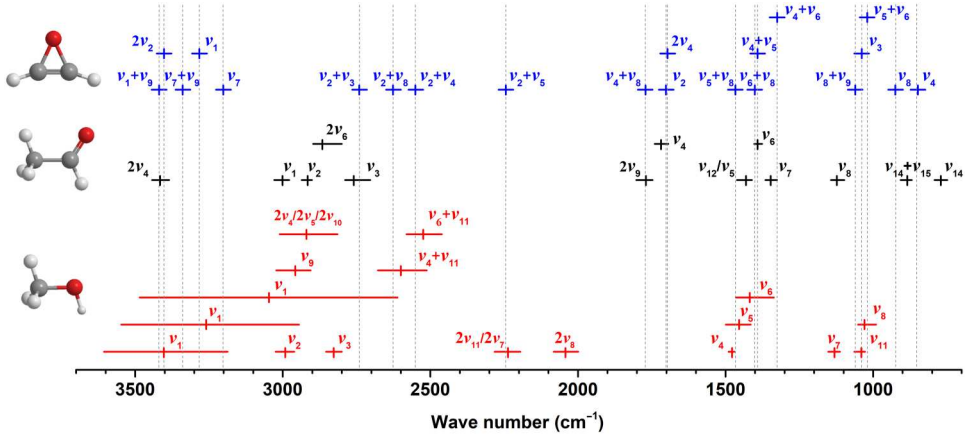

Fig. 3. Peak absorptions (solid vertical lines) and absorption ranges (solid horizontal lines) of methanol (CH_3OH, red), acetaldehyde (CH_3CHO, black), and oxirene (*c*-C_2H_2O, blue). Dotted vertical lines indicate the overlap between the absorption peaks of oxirene and reactants (CH_3OH, red; CH_3CHO, black). Detailed absorptions and assignments for experimentally measured pure methanol and acetaldehyde ices as well as calculated oxirene are listed in table S4.

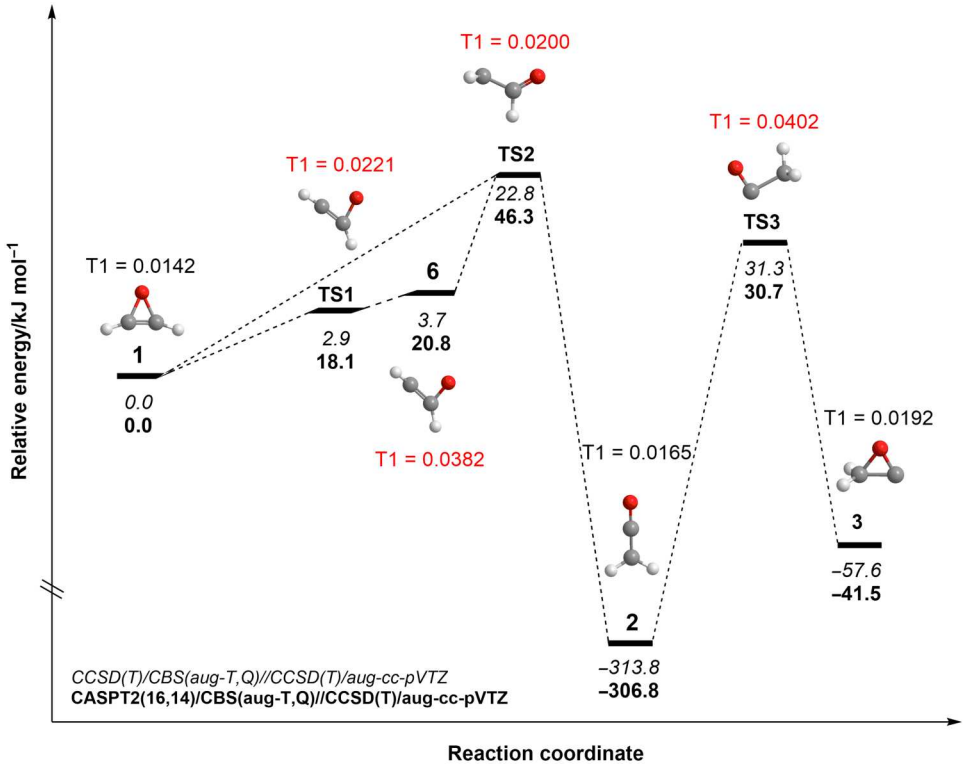

Fig. 4. Potential energy profile of the reaction coordinate from oxirene (1) to ketene (2). Singlet formylcarbene (**6**) optimizes as a local minimum; however, the inclusion of ZPE lifts its energy above the energy of the transition state separating it from oxirene (**1**). See text for details.

DISCUSSION

To conclude, the present study presents the first preparation of the hitherto elusive oxirene (*c*-C_2H_2O, **1**) molecule—the prototype of a highly strained, 4π Hückel antiaromatic heterocyclic organic molecule in low-temperature methanol-acetaldehyde ices and detection in the gas phase exploiting isomer-selective soft PI-ReTOF-MS. Upon formation through isomerization of ketene (H_2CCO, **2**), oxirene (**1**) is stabilized in the matrix via resonances with the vibrational modes of the matrix molecule (methanol). The transfer rate of newly formed vibrationally excited molecules [oxirene (**1**)] in the matrix (methanol) maximizes when the vibrational frequencies of the donor [oxirene (**1**)] and acceptor molecules (methanol) are at resonance, i.e., have identical frequencies (*47*). This is the case for the oxirene-methanol system as demonstrated in Fig. 3 and figs. S6 to S8. Oxirene is photolabile as demonstrated in a UV photolysis experiment. The thermal sublimation of the molecules from the ices is well represented by a Maxwell-Boltzmann distribution. Taking the average molecular velocity of 254 m s^{-1} for oxirene (**1**) subliming at an average temperature of 129 K along with the distance between the ice surface and the photoionization region of 2.0 ± 0.5 mm, the lifetime of the neutral oxirene (**1**) in the gas phase has to exceed 8 ± 2 μs, while the corresponding molecular ions have to survive at least 29 ± 1 μs before they reach the detector of the ReTOF-MS. The principle of deactivation of matrix isolated energetic (internally excited) transients due to resonance vibrational energy transfer in the matrix opens the door for the synthesis of highly strained organics such as 1H-phosphirene (*c*-C_2H_2PH)—the isovalent counterpart of oxirene (**1**)—organic chemists have attempted to prepare in the laboratory for decades and predicts that oxirene (**1**) is likely synthesized in methanol-rich interstellar ices in cold molecular clouds from acetaldehyde followed by sublimation in the hot core stage such as of Sagittarius B2 (Sgr B2), thus manifesting molecular clouds and star-forming regions as natural laboratories on a macroscopic scale harboring exotic organics in deep space (*48*–*50*).

MATERIALS AND METHODS

Experimental methods

All experiments were carried out in a stainless steel ultrahigh vacuum chamber evacuated to a few 10^{-11} torr by magnetically levitated turbomolecular pumps (Osaka Vacuum, TG1300MUCWB and TG420MCAB) backed by an oil-free scroll pump (Edwards Vacuum, GVSP30). A polished silver substrate was interfaced to a cold head and was cooled to 5 K by a closed-cycle helium compressor (Sumitomo Heavy Industries, RDK-415E). The silver substrate can be translated vertically and rotated in the horizontal plane. After the wafer reached 5 K, methanol (CH_3OH, Sigma-Aldrich, high-performance liquid chromatography grade) and acetaldehyde (CH_3CHO, Sigma-Aldrich, anhydrous, ≥99.5% purity) were co-deposited onto the wafer by introducing each reactant to the chamber at a pressure of 2×10^{-8} torr via separate glass capillary arrays. Isotopically labeled methanol (CD_3OH, Sigma-Aldrich, ≥98 atom % D) and isotopically labeled acetaldehyde (CD_3CHO, CDN isotopes, ≥98 atom % D; CD_3CDO, Sigma-Aldrich, ≥99 atom % D; $^{13}CH_3{}^{13}CHO$, Sigma-Aldrich, 99 atom % ^{13}C) were used in duplicate experiments to observe mass shifts of products. Laser interferometry was used to determine the thickness of the ice based on the

interference pattern produced by helium: neon laser (CVI Melles Griot; 25-LHP-230; 632.8 nm) reflected off the surface at an angle of 2° relative to the ice surface normal (*51*). By averaging the refractive indexes of pure amorphous methanol ice ($n = 1.33 \pm 0.04$) (*52*) and that of acetaldehyde ($n = 1.303$) (*53*), the ice thickness was calculated to be 740 ± 40 nm; this is thicker than the average penetration depth of the electrons (330 ± 20 nm), which excludes interactions of the electrons with the substrate. The ice composition ratio of methanol to acetaldehyde was determined to be 1.0 ± 0.3:1 by integrating the infrared features of methanol at 2825 cm^{-1} (ν_3) and 3261 cm^{-1} (ν_1) and acetaldehyde at 1122 cm^{-1} (ν_8) and 1345 cm^{-1} (ν_7), which have absorption coefficients of 5.3×10^{-18}, 1.01×10^{-16}, 6.6×10^{-19}, and 1.1×10^{-18} cm $molecule^{-1}$, respectively (*39*, *52*, *54*, *55*).

After deposition, the samples were irradiated with 5-keV electrons at a current of 20 nA for 15 or 60 min, which corresponds to doses of up to 2.5 eV $molecule^{-1}$ for methanol and 3.8 eV $molecule^{-1}$ for acetaldehyde, respectively, for 20 nA (60 min) according to CASINO simulations (*56*). An additional photolysis experiment at 304 nm for 5 hours was performed after the electron irradiation to photolyze synthesized oxirene. Infrared spectra (6000 to 500 cm^{-1}) of the ices were collected before, during, and after the irradiation or photolysis to track changes in the chemical composition using an FTIR (Thermo Nicolet 6700) spectrometer with 4 cm^{-1} spectral resolution. During the irradiation, FTIR spectra of the ices were recorded every 2 min. The FTIR spectra of the pristine ice are shown in figs. S1 and S2. Detailed assignments of the peaks are compiled in tables S1 and S2.

After the irradiation, the ices were heated from 5 to 320 K at a rate of 0.5 K min^{-1} (TPD) or first photolyzed by 304-nm light at 20 mW for 5 hours and then heated to 320 K at 0.5 K min^{-1} by a programmable temperature controller (Lakeshore 336). The 304-nm laser light was generated by frequency doubling of 608-nm light, which was produced by using the second harmonic (532 nm) of a pulsed neodymium-doped yttrium aluminum garnet laser (Nd: YAG, Spectra-Physics, PRO-270, 30 Hz) to pump the Rhodamine 610/640 dye mixture. During the TPD phase, the sublimed molecules from the sample were analyzed by VUV PI-ReTOF-MS. The VUV photons at 9.70, 9.20, and 8.25 eV were generated by resonant four-wave mixing (FWM) of two synchronized pulsed laser beams from two dye lasers (Sirah, Cobra-Stretch) pumped by two Nd: YAG lasers (table S10). To produce 9.70-eV light, the Rhodamine 610/640 dye mixture was pumped by the second harmonic (532 nm) of an Nd: YAG laser to obtain 606.948 nm, which produces ω_1 = 202.316 nm via third harmonic generation. The Coumarin 480 dye was pumped by a second Nd: YAG laser to obtain ω_2 = 484.982 nm, which then generated 9.70-eV photons in krypton gas by combining with $2\omega_1$. To generate 9.20- and 8.25-eV photons, xenon gas was used as a nonlinear medium. The 9.20-eV light was generated by the difference FWM in pulsed gas jets of xenon gas with ω_1 = 222.566 nm and ω_2 = 638.667 nm, which were obtained via a double frequency of 445.132 nm from Coumarin 450 dye pumped by the third harmonic (355 nm) of an Nd: YAG laser and via 4-(dicyanomethylene)-2-methyl-6-(4-dimethylaminostyryl)-4H-pyran dye in dimethyl sulfoxide pumped by the second harmonic of an Nd: YAG laser, respectively. For 8.25 eV, ω_1 = 249.628 nm and ω_2 = 736.448 nm are used. The ω_1 = 249.628 nm was obtained via a double frequency of 499.256 nm from Coumarin 503 dye pumped by an Nd: YAG laser. While the ω_2 = 736.448 nmwas generated from LDS (laser dye) 722 dye. The VUV light was spatially separated from other wavelengths (ω_1; ω_2; $2\omega_1 + \omega_2$; $3\omega_1$; $3\omega_2$) using a biconvex lithium fluoride (LiF) lens (ISP Optics) in an off-axis geometry and then directed at 2.0 ± 0.5 mm above the substrate surface to ionize subliming molecules during the TPD phase. The resulting molecular ions were mass analyzed with a ReTOF mass spectrometer (Jordan TOF Products Inc.). The signals were amplified by a preamplifier (Ortec 9305), shaped with a 100-MHz discriminator (F-100TD, Advanced Research Instruments Corporation), and recorded by a multichannel scaler (FAST ComTec, MCS6A) with accumulation times of 2 min (3600 sweeps) at 30 Hz for each recorded mass spectra in 0.5 K min^{-1} during the TPD phase.

Computational methods

All density functional theory (DFT) computations were carried out with Gaussian 16, Revision C.01 (*57*). For geometry optimizations and frequency computations, initially the DFT PBE0 functional (*58*–*60*) was employed using the Dunning correlation consistent split valence basis set (aug-cc-pVTZ) (*61*). All coupled-cluster computations were carried out with the CFOUR program package (*62*). In general, the coupled-cluster level of theory within the frozen core approximation including single, double, and perturbatively included triple excitations [CCSD(T)] (*63*–*65*) using the aug-cc-pVTZ (*66*) basis set was used for the final geometry optimizations and frequency calculations. To determine the nature of all stationary points, we computed the corresponding frequencies (no imaginary frequencies for minima and exactly one imaginary frequency for transition states). On the basis of these geometries, the corresponding frozen-core coupled-cluster (*63*–*65*, *67*) CCSD(T)/aug-cc-pVTZ and CCSD(T)/aug-cc-pVQZ single-point energies were computed using the built-in extrapolation routine in ORCA 5.0.3 (*68*) and extrapolated to CBS limit (*69*) CCSD(T)/CBS(aug-T,Q) with CCSD(T)/aug-cc-pVTZ harmonic zero-point vibrational energies (ZPVEs) and PBE0/aug-cc-pVTZ anharmonic ZPVE corrections. The adiabatic IEs were computed by taking the ZPVE corrected energy difference between the neutral and ionic species that correspond to similar conformations. As in general the difference between heavier isotopologues and standard isotopologues in the ZPVE is marginal, we used the ZPVEs of standard isotopologues for IE calculation and assume them as the same for our experiments with heavier isotopologues. The calculated accuracy is within 0.01 eV for IE in comparison with the measured experimental IE of ketene (**2**) (table S5). Computed Cartesian coordinates and vibration frequencies are listed in table S11. The UV-Vis spectra for oxirene (**1**) and ketene (**2**) were calculated at the TD-PBE0/cc-pVTZ level of theory (fig. S4). CASPT2 calculations were carried out using the MOLPRO 2021 package (*70*).

Supplementary Materials

This PDF file includes:

Figs. S1 to S9
Tables S1 to S11
References

REFERENCES AND NOTES

1. M. Berthelot, Nouvelle méthode de synthèse des acides organiques. *Bull. Soc. Chim. Fr.* 14, 113–119 (1870).

2. E. G. Lewars, in *Modeling Marvels: Computational Anticipation of Novel Molecules* (Springer Netherlands, 2008), pp. 31–52.
3. S. J. Klippenstein, L. B. Harding, B. Ruscic, Ab initio computations and active thermochemical tables hand in hand: Heats of formation of core combustion species. *J. Phys. Chem. A* **121**, 6580–6602 (2017).
4. I. G. Csizmadia, J. Font, O. P. Strausz, Mechanism of the Wolff rearrangement. *J. Am. Chem. Soc.* **90**, 7360–7361 (1968).
5. S. A. Matlin, P. G. Sammes, Decomposition of α-diazo-ketones: The oxiren–oxocarbene equilibrium. *J. Chem. Soc. Perkin Trans.* **1**, 2623–2630 (1972).
6. J. F. Liebman, A. Greenberg, A survey of strained organic molecules. *Chem. Rev.* **76**, 311–365 (1976).
7. R. C. Mawhinney, J. D. Goddard, Assessment of density functional theory for the prediction of the nature of the oxirene stationary point. *J. Mol. Struct. Theochem* **629**, 263–270 (2003).
8. E. Lewars, Benzooxirene. Ab initio calculations. *J. Mol. Struct. Theochem* **360**, 67–80 (1996).
9. O. P. Strausz, R. K. Gosavi, A. S. Denes, I. G. Csizmadia, Mechanism of the Wolff rearrangement. 6. Ab initio molecular orbital calculations on the thermodynamic and kinetic stability of the oxirene molecule. *J. Am. Chem. Soc.* **98**, 4784–4786 (1976).
10. C. Bachmann, T. Y. N'Guessan, F. Debu, M. Monnier, J. Pourcin, J. P. Aycard, H. Bodot, Oxirenes and ketocarbenes from α-diazoketone photolysis: Experiments in rare gas matrices. Relative stabilities and isomerization barriers from MNDOC-BWEN calculations. *J. Am. Chem. Soc.* **112**, 7488–7497 (1990).
11. F. Turecek, D. E. Drinkwater, F. W. McLafferty, Gas-phase formation and rearrangements of methyloxirene and its cation radical. *J. Am. Chem. Soc.* **113**, 5958–5964 (1991).
12. W. J. Bouma, R. H. Nobes, L. Radom, C. Woodward, Existence of stable structural isomers of ketene. A theoretical study of the C_2H_2O potential energy surface. *J. Org. Chem.* **47**, 1869–1875 (1982).
13. A. P. Scott, R. H. Nobes, H. F. Schaefer, L. Radom, The Wolff rearrangement: The relevant portion of the oxirene-ketene potential energy hypersurface. *J. Am. Chem. Soc.* **116**, 10159–10164 (1994).
14. W. Kirmse, 100 years of the Wolff rearrangement. *Eur. J. Org. Chem.* **2002**, 2193–2256 (2002).
15. M. Torres, J. L. Bourdelande, A. Clement, O. P. Strausz, Argon-matrix isolation of bis(-trifluoromethyl)oxirene, perfluoromethylethyloxirene, and their isomeric ketocarbenes. *J. Am. Chem. Soc.* **105**, 1698–1700 (1983).
16. P. Carsky, B. A. Hess Jr., L. J. Schaad, Ab initio study of the structures and vibrational spectra of the Hueckel 4n heterocycles azirine, oxirene and thiirene. *J. Am. Chem. Soc.* **105**, 396–402 (1983).
17. G. Vacek, J. M. Galbraith, Y. Yamaguchi, H. F. Schaefer, R. H. Nobes, A. P. Scott, L. Radom, Oxirene: To be or not to be? *J. Phys. Chem.* **98**, 8660–8665 (1994).
18. P. J. Wilson, D. J. Tozer, A Kohn-Sham study of the oxirene-ketene potential energy surface. *Chem. Phys. Lett.* **352**, 540–544 (2002).
19. E. G. Lewars, in *Computational Chemistry: Introduction to the Theory and Applications of Molecular and Quantum Mechanics* (Springer International Publishing, 2016), pp. 613–643.
20. A. Rey Planells, A. Espinosa Ferao, Accurate ring strain energies of unsaturated three-membered heterocycles with one group 13–16 element. *Inorg. Chem.* **61**, 6459–6468 (2022).
21. A. Karton, D. Talbi, Pinning the most stable $H_xC_yO_z$ isomers in space by means of high-level theoretical procedures. *Chem. Phys.* **436-437**, 22–28 (2014).
22. M. Torres, A. Clement, O. P. Strausz, Photolysis of vinylene thioxocarbonates: A new source of ketocarbenes. *J. Org. Chem.* **45**, 2271–2273 (1980).
23. C. E. C. A. Hop, J. L. Holmes, J. K. Terlouw, The oxirene radical cation and its neutralization in the gas phase. *J. Am. Chem. Soc.* **111**, 441–445 (1989).
24. R. Hochstrasser, J. Wirz, Reversible photoisomerization of ketene to ethynol. *Angew. Chem. Int. Ed.* **29**, 411–413 (1990).
25. J. P. Toscano, M. S. Platz, V. Nikolaev, Lifetimes of simple ketocarbenes. *J. Am. Chem. Soc.* **117**, 4712–4713 (1995).
26. J. P. Toscano, M. S. Platz, V. Nikolaev, Y. Cao, M. B. Zimmt, The lifetime of formylcarbene determined by transient absorption and transient grating spectroscopy. *J. Am. Chem. Soc.* **118**, 3527–3528 (1996).
27. A. M. Turner, R. I. Kaiser, Exploiting photoionization reflectron time-of-flight mass spectrometry to explore molecular mass growth processes to complex organic molecules in interstellar and solar system ice analogs. *Acc. Chem. Res.* **53**, 2791–2805 (2020).
28. A. M. Turner, A. S. Koutsogiannis, N. F. Kleimeier, A. Bergantini, C. Zhu, R. C. Fortenberry, R. I. Kaiser, An experimental and theoretical investigation into the formation of ketene (H_2CCO) and ethynol (HCCOH) in interstellar analog ices. *Astrophys. J.* **896**, 88 (2020).
29. S. Maity, R. I. Kaiser, B. M. Jones, Formation of complex organic molecules in methanol and methanol–carbon monoxide ices exposed to ionizing radiation—A combined FTIR and reflectron time-of-flight mass spectrometry study. *Phys. Chem. Chem. Phys.* **17**, 3081–3114 (2015).
30. N. F. Kleimeier, A. M. Turner, R. C. Fortenberry, R. I. Kaiser, On the formation of the popcorn flavorant 2,3-butanedione ($CH_3COCOCH_3$) in acetaldehyde-containing interstellar ices. *ChemPhysChem* **21**, 1531–1540 (2020).
31. R. L. Hudson, M. J. Loeffler, Ketene formation in interstellar ices: A laboratory study. *Astrophys. J.* **773**, 109 (2013).
32. G. Maier, H. P. Reisenauer, M. Cibulka, Oxiranylidene. *Angew. Chem. Int. Ed.* **38**, 105–108 (1999).
33. P. J. Linstrom, W. G. Mallard, NIST Chemistry WebBook, *NIST Standard Reference Database Number 69, Natl. Inst. Stand. Technol.* (2013); http://webbook.nist.gov/.
34. M. J. Abplanalp, R. I. Kaiser, On the formation of complex organic molecules in the interstellar medium: Untangling the chemical complexity of carbon monoxide-hydrocarbon containing ice analogues exposed to ionizing radiation via a combined infrared and reflectron time-of-flight analysis. *Phys. Chem. Chem. Phys.* **21**, 16949–16980 (2019).
35. S. Maity, R. I. Kaiser, B. M. Jones, Infrared and reflectron time-of-flight mass spectroscopic study on the synthesis of glycolaldehyde in methanol (CH_3OH) and methanol–carbon monoxide (CH_3OH–CO) ices exposed to ionization radiation. *Faraday Discuss.* **168**, 485–516 (2014).
36. S. Kobatake, S. Takami, H. Muto, T. Ishikawa, M. Irie, Rapid and reversible shape changes of molecular crystals on photoirradiation. *Nature* **446**, 778–781 (2007).
37. M. Irie, T. Fukaminato, T. Sasaki, N. Tamai, T. Kawai, A digital fluorescent molecular photoswitch. *Nature* **420**, 759–760 (2002).
38. D. Mei, A. M. Karim, Y. Wang, On the reaction mechanism of acetaldehyde decomposition on Mo (110). *ACS Catal.* **2**, 468–478 (2012).
39. N. F. Kleimeier, A. K. Eckhardt, R. I. Kaiser, A mechanistic study on the formation of acetic acid (CH_3COOH) in polar interstellar analog ices exploiting photoionization reflectron time-of-flight mass spectrometry. *Astrophys. J.* **901**, 84 (2020).
40. C.-S. Lam, J. D. Adams, L. J. Butler, The onset of H^+ ketene products from vinoxy radicals prepared by photodissociation of chloroacetaldehyde at 157 nm. *J. Phys. Chem. A* **120**, 2521–2536 (2016).
41. V. Saheb, S. R. Hashemi, S. M. A. Hosseini, Theoretical studies on the kinetics of multi-channel gas-phase unimolecular decomposition of acetaldehyde. *J. Phys. Chem. A* **121**, 6887–6895 (2017).
42. J. Guan, K. R. Randall, H. F. Schaefer III, H. Li, Formylmethylene: The triplet ground state and the lowest singlet state. *J. Phys. Chem. A* **117**, 2152–2159 (2013).
43. T. J. Lee, P. R. Taylor, A diagnostic for determining the quality of single-reference electron correlation methods. *Int. J. Quantum Chem.* **36**, 199–207 (1989).
44. P. Celani, H.-J. Werner, Multireference perturbation theory for large restricted and selected active space reference wave functions. *J. Chem. Phys.* **112**, 5546–5557 (2000).
45. T. Shiozaki, W. Győrffy, P. Celani, H.-J. Werner, Communication: Extended multi-state complete active space second-order perturbation theory: Energy and nuclear gradients. *J. Chem. Phys.* **135**, 081106 (2011).
46. D. J. Goebbert, D. Khuseynov, A. Sanov, O^- + acetaldehyde reaction products: Search for singlet formylmethylene, a Wolff rearrangement intermediate. *J. Phys. Chem. A* **115**, 3208–3217 (2011).
47. J. Cao, Generalized resonance energy transfer theory: Applications to vibrational energy flow in optical cavities. *J. Phys. Chem. Lett.* **13**, 10943–10951 (2022).
48. M. J. Barlow, B. M. Swinyard, P. J. Owen, J. Cernicharo, H. L. Gomez, R. J. Ivison, O. Krause, T. L. Lim, M. Matsuura, S. Miller, G. Olofsson, E. T. Polehampton, Detection of a noble gas molecular ion, $^{36}ArH^+$, in the Crab Nebula. *Science* **342**, 1343–1345 (2013).
49. J. Cernicharo, C. Kahane, J. Gomez-Gonzalez, M. Guelin, Tentative detection of the C_5H radical. *Astron. Astrophys.* **164**, L1–L4 (1986).
50. L. N. Zack, D. T. Halfen, L. M. Ziurys, Detection of FeCN ($X^4\Delta_i$) in IRC+10216: A new interstellar molecule. *Astrophys. J.* **733**, L36 (2011).
51. A. M. Turner, M. J. Abplanalp, S. Y. Chen, Y. T. Chen, A. H. Chang, R. I. Kaiser, A photoionization mass spectroscopic study on the formation of phosphanes in low temperature phosphine ices. *Phys. Chem. Chem. Phys.* **17**, 27281–27291 (2015).
52. M. Bouilloud, N. Fray, Y. Benilan, H. Cottin, M. C. Gazeau, A. Jolly, Bibliographic review and new measurements of the infrared band strengths of pure molecules at 25 K: H_2O, CO_2, CO, CH_4, NH_3, CH_3OH, HCOOH and H_2CO. *Mon. Not. R. Astron. Soc.* **451**, 2145–2160 (2015).
53. R. L. Hudson, F. M. Coleman, Infrared intensities and molar refraction of amorphous dimethyl carbonate—Comparisons to four interstellar molecules. *Phys. Chem. Chem. Phys.* **21**, 11284–11289 (2019).
54. D. M. Hudgins, S. A. Sandford, L. J. Allamandola, A. G. Tielens, Mid- and far-infrared spectroscopy of ices: Optical constants and integrated absorbances. *Astrophys. J. Suppl. Ser.* **86**, 713–870 (1993).
55. C. Zhu, A. M. Turner, C. Meinert, R. I. Kaiser, On the production of polyols and hydroxycarboxylic acids in interstellar analogous ices of methanol. *Astrophys. J.* **889**, 134 (2020).

56. D. Drouin, A. R. Couture, D. Joly, X. Tastet, V. Aimez, R. Gauvin, CASINO V2.42—A fast and easy-to-use modeling tool for scanning electron microscopy and microanalysis users. *Scanning* **29**, 92–101 (2007).
57. M. J. Frisch, G. W. Trucks, H. B. Schlegel, G. E. Scuseria, M. A. Robb, J. R. Cheeseman, G. Scalmani, V. Barone, G. A. Petersson, H. Nakatsuji, X. Li, M. Caricato, A. V. Marenich, J. Bloino, B. G. Janesko, R. Gomperts, B. Mennucci, H. P. Hratchian, J. V. Ortiz, A. F. Izmaylov, J. L. Sonnenberg, Williams, F. Ding, F. Lipparini, F. Egidi, J. Goings, B. Peng, A. Petrone, T. Henderson, D. Ranasinghe, V. G. Zakrzewski, J. Gao, N. Rega, G. Zheng, W. Liang, M. Hada, M. Ehara, K. Toyota, R. Fukuda, J. Hasegawa, M. Ishida, T. Nakajima, Y. Honda, O. Kitao, H. Nakai, T. Vreven, K. Throssell, J. A. Montgomery Jr., J. E. Peralta, F. Ogliaro, M. J. Bearpark, J. J. Heyd, E. N. Brothers, K. N. Kudin, V. N. Staroverov, T. A. Keith, R. Kobayashi, J. Normand, K. Raghavachari, A. P. Rendell, J. C. Burant, S. S. Iyengar, J. Tomasi, M. Cossi, J. M. Millam, M. Klene, C. Adamo, R. Cammi, J. W. Ochterski, R. L. Martin, K. Morokuma, O. Farkas, J. B. Foresman, D. J. Fox, *Gaussian 16* (Gaussian Inc., 2016).
58. A. D. Becke, Density-functional exchange-energy: Approximation with correct asymptotic behavior. *Phys. Rev. A* **38**, 3098–3100 (1988).
59. C. Lee, W. Yang, R. G. Parr, Development of the Colle-Salvetti correlation-energy formula into a functional of the electron density. *Phys. Rev. B* **37**, 785–789 (1988).
60. A. D. Becke, Density-functional thermochemistry. III. The role of exact exchange. *J. Chem. Phys.* **98**, 5648–5652 (1993).
61. T. H. Dunning, Gaussian basis sets for use in correlated molecular calculations. I. The atoms boron through neon and hydrogen. *J. Chem. Phys.* **90**, 1007–1023 (1989).
62. D. A. Matthews, L. Cheng, M. E. Harding, F. Lipparini, S. Stopkowicz, T.-C. Jagau, P. G. Szalay, J. Gauss, J. F. Stanton, Coupled-cluster techniques for computational chemistry: The CFOUR program package. *J. Chem. Phys.* **152**, 214108 (2020).
63. J. Čížek, On the correlation problem in atomic and molecular systems. Calculation of wavefunction components in Ursell-type expansion using quantum-field theoretical methods. *J. Chem. Phys.* **45**, 4256–4266 (1966).
64. K. Raghavachari, Electron correlation techniques in quantum chemistry: Recent advances. *Annu. Rev. Phys. Chem.* **42**, 615–642 (1991).
65. R. J. Bartlett, J. D. Watts, S. A. Kucharski, J. Noga, Non-iterative fifth-order triple and quadruple excitation energy corrections in correlated methods. *Chem. Phys. Lett.* **165**, 513–522 (1990).
66. R. A. Kendall, T. H. Dunning Jr., R. J. Harrison, Electron affinities of the first-row atoms revisited. Systematic basis sets and wave functions. *J. Chem. Phys.* **96**, 6796–6806 (1992).
67. J. F. Stanton, Why CCSD(T) works: A different perspective. *Chem. Phys. Lett.* **281**, 130–134 (1997).
68. F. Neese, Software update: The ORCA program system, version 4.0. *WIREs Comput. Mol. Sci.* **8**, e1327 (2018).
69. K. A. Peterson, D. E. Woon, T. H. Dunning Jr., Benchmark calculations with correlated molecular wave functions. IV. The classical barrier height of the $H+H_2 \rightarrow H_2+H$ reaction. *J. Chem. Phys.* **100**, 7410–7415 (1994).
70. H.-J. Werner, P. J. Knowles, G. Knizia, F. R. Manby, M. Schütz, P. Celani, W. Györffy, D. Kats, T. Korona, R. Lindh, A. Mitrushenkov, G. Rauhut, K. R. Shamasundar, T. B. Adler, R. D. Amos, S. J. Bennie, A. Bernhardsson, A. Berning, D. L. Cooper, M. J. O. Deegan, A. J. Dobbyn, F. Eckert, E. Goll, C. Hampel, A. Hesselmann, G. Hetzer, T. Hrenar, G. Jansen, C. Köppl, S. J. R. Lee, Y. Liu, A. W. Lloyd, Q. Ma, R. A. Mata, A. J. May, S. J. McNicholas, W. Meyer, T. F. Miller III, M. E. Mura, A. Nicklass, D. P. O'Neill, P. Palmieri, D. Peng, T. Petrenko, K. Pflüger, R. Pitzer, M. Reiher, T. Shiozaki, H. Stoll, A. J. Stone, R. Tarroni, T. Thorsteinsson, M. Wang, and M. Welborn, MOLPRO, version 2021.2. A package of ab initio programs (University of Cardiff, 2021); www.molpro.net.
71. N. F. Kleimeier, A. K. Eckhardt, R. I. Kaiser, Identification of glycolaldehyde enol (HOHC═CHOH) in interstellar analogue ices. *J. Am. Chem. Soc.* **143**, 14009–14018 (2021).
72. N. F. Kleimeier, R. I. Kaiser, Interstellar enolization-acetaldehyde (CH_3CHO) and vinyl alcohol ($H_2CCH(OH)$) as a case study. *ChemPhysChem* **22**, 1229–1236 (2021).
73. C. Zhu, N. F. Kleimeier, A. M. Turner, S. K. Singh, R. C. Fortenberry, R. I. Kaiser, Synthesis of methanediol [$CH_2(OH)_2$]: The simplest geminal diol. *Proc. Natl. Acad. Sci. U.S.A.* **119**, e2111938119 (2022).
74. C. Zhu, R. Frigge, A. Bergantini, R. C. Fortenberry, R. I. Kaiser, Untangling the formation of methoxymethanol (CH_3OCH_2OH) and dimethyl peroxide (CH_3OOCH_3) in star-forming regions. *Astrophys. J.* **881**, 156 (2019).

Acknowledgments

Funding: This work was supported by the U.S. National Science Foundation, Division of Astronomical Sciences under grant AST-2103269 awarded to the University of Hawaii at Manoa (to R.I.K.). A.K.E. thanks the Fonds der Chemischen Industrie (Liebig Fellowship) and the Deutsche Forschungsgemeinschaft (DFG, German Research Foundation) under Germany's Excellence Strategy–EXC-2033–390677874–RESOLV for funding. **Author contributions:** R.I.K. designed the experiments. J.W., J.H.M., and A.M.T. performed experiments and analyzed the data. A.K.E. and A.M.M. carried out the theoretical analysis. J.W., A.K.E., and R.I.K. wrote the manuscript, which was read, revised, and approved by all coauthors. **Competing interests:** The authors declare that they have no competing interests. **Data and materials availability:** All data needed to evaluate the conclusions in the paper are present in the paper and/or the Supplementary Materials.

Submitted 2 December 2022
Accepted 8 February 2023
Published 10 March 2023
10.1126/sciadv.adg1134